Mesophase separation and probe dynamics in protein–polyelectrolyte coacervates†

A. Basak Kayitmazer,*[a] Himadri B. Bohidar,[b] Kevin W. Mattison,‡[g] Arijit Bose,[c] Jayashri Sarkar,[c] Akihito Hashidzume,[d] Paul S. Russo,[e] Werner Jaeger[f] and Paul L. Dubin[a]

Received 29th January 2007, Accepted 24th May 2007
First published as an Advance Article on the web 25th June 2007
DOI: 10.1039/b701334e

Protein–polyelectrolyte coacervates are self-assembling macroscopically monophasic biomacromolecular fluids whose unique properties arise from transient heterogeneities. The structures of coacervates formed at different conditions of pH and ionic strength from poly(dimethyldiallylammonium chloride) and bovine serum albumin (BSA), were probed using fluorescence recovery after photobleaching. Measurements of self-diffusion in coacervates were carried out using fluorescein-tagged BSA, and similarly tagged Ficoll, a non-interacting branched polysaccharide with the same size as BSA. The results are best explained by temporal and spatial heterogeneities, also inferred from static light scattering and cryo-TEM, which indicate heterogeneous scattering centers of several hundred nm. Taken together with previous dynamic light scattering and rheology studies, the results are consistent with the presence of extensive dilute domains in which are embedded partially interconnected 50–700 nm dense domains. At short length scales, protein mobility is unobstructed by these clusters. At intermediate length scales, proteins are slowed down due to tortuosity effects within the blind alleys of the dense domains, and to adsorption at dense/dilute domain interfaces. Finally, at long length scales, obstructed diffusion is alleviated by the break-up of dense domains. These findings are discussed in terms of previously suggested models for protein–polyelectrolyte coacervates. Possible explanations for the origin of mesophase separation are offered.

Introduction

Protein–polyelectrolyte (PE) coacervates[1–5] are dense, macromolecule-rich liquid phases formed by liquid–liquid phase separation from mixtures of the two macroions. Polyelectrolyte complex coacervation, in general, is thought to be driven by electrostatic attractive forces and by the entropy gain coming from the release of small ions.[6–8] Motivations for investigating protein–PE coacervates are quite diverse. Oparin[9] suggested coacervates as a model for precellular structures, partly because the absence of aggregation at high protein concentrations (>20% w/w) is characteristic of both coacervates and the intracellular environment. Several applications of protein–PE coacervates have been utilized or proposed. First, protein–PE coacervation has long been used to microencapsulate oil droplets,[10,11] protein drugs[12,13] and enzymes.[14] Second, polyelectrolyte coacervation can be used to separate proteins, even those with similar pI.[15] Third, the preservation of enzyme activity in 20–25% enzyme-loaded coacervate droplets[16] points to their use as enzyme microreactors.[17] These considerations motivate a deeper understanding of both the mechanism of protein–PE coacervation and the nature of the coacervates.

Intermacroionic complex coacervation broadly includes not only coacervation of proteins and PEs, and the closely related cases of PEs and micelles[6,18] and PEs and dendrimers,[19] but also and more commonly, coacervation between oppositely charged random coil PEs.[20–23] The former are examples of "PE–colloid" coacervation and might in some sense be distinct from PE–PE coacervation, which includes both purely synthetic systems but more typically PE's of natural origin such as gum acacia (gum Arabic) and gelatin. Theories for complex coacervation of such statistical chain PEs might be relevant to protein–PE coacervation, but it is necessary to consider whether phenomenological results support this suggestion. While comparison of PE–PE coacervates to PE–protein coacervates is impeded by the lack of parity in experimental conditions and procedures, some generalizations serve to illustrate similarities.

(i) Coacervation is suppressed at high salt concentration. Salt suppression of coacervation is common to both PE–PE and

[a]*Department of Chemistry, University of Massachusetts Amherst, 710 N. Pleasant St. LGRT 701 Amherst, MA 01003, USA. E-mail: akayitma@chem.umass.edu*
[b]*School of Physical Sciences, Jawaharlal Nehru University, India*
[c]*Department of Chemical Engineering, University of Rhode Island, Kingston, RI, USA*
[d]*Department of Macromolecular Science, Osaka University, Japan*
[e]*Department of Chemistry, Louisiana State University, USA*
[f]*Fraunhofer Institute of Applied Polymer Research, Germany*
[g]*Department of Chemistry, Indiana University–Purdue University, Indianapolis, IN, USA*
† The HTML version of this article has been enhanced with colour images.
‡ *Present address*: Malvern Instruments, MA, USA.

PE–protein systems and is clearly a result of screening of electrostatic forces. This is most evident when highly turbid coacervate suspensions of gelatin/gum acacia or gelatin/chitosan become optically clear upon addition of NaCl above *e.g.* 50 mM.[20,24,25] Coacervates of bovine serum albumin (BSA) and polydiallyldimethylammonium chloride (PDADMAC) can dissociate into soluble complexes with an increase in salt concentration at a fixed pH.[26] ''Partial suppression'' at low salt reported[24] based on ''coacervate yield'' might reflect coacervate composition rather than coacervate thermodynamic stability. Low salt suppression, if it exists, could arise from repulsions among weakly charged soluble complexes.

(ii) Soluble complexes are precursors of coacervation. Systematic studies of PE–protein complex formation by Dubin and co-workers have shown that coacervate formation is preceded by soluble complex formation.[27] While there are few studies that address the question of soluble complexes as precursors of PE–PE coacervation, such complexes (''ionic aggregates'') have also been reported in the dilute phase for coacervates of gelatin A (pI = 9) with gelatin B (pI = 5).[28]

(iii) The composition of the condensed (coacervate) phase can be fixed or may depend on the mixing ratio. For both protein–PE and PE–PE, coacervate stoichiometry depends on macroion complementarity and salt concentration. Intermacroionic phase separation in the absence of salt leads to dense phases of well-defined stoichiometry arising from the requirement of charge neutrality $N_{pr}Z_{pr}/N_PZ_P = 1 = \rho$ for protein–PE systems, where N and Z are the number concentration and molecular charge of protein and PE in the dense phase. Simulations by Skepoe and Linse[29] indicated phase separation occurring at macromolecular charge equivalence in the absence of salt, in agreement with findings by Kokufuta *et al.*[30] for a number of PE's precipitating with human serum albumin in pure water. Non-stoichiometric PDADMAC–BSA coacervates are formed in 50 mM NaCl.[31] Non-stoichiometric coacervation was also found by Sato and Nakajima[32] in salt-free mixtures of a weak rigid polyanion, carboxymethyl cellulose, with a flexible weak polycation, polyethylenimine. Non-stoichiometry, *i.e.* macromolecular charge imbalance, implies that charge neutrality cannot be achieved by complementarity of the two macroions, thus requiring compensation by small ions. This is likely to be the case for macroion pairs that are highly asymmetric with respect to macroion charge density or chain flexibility. The possibility of non-stoichiometry is also enhanced by the presence of salt which provides compensating small ions without a large ionic strength difference between the two phases.

(iv) For both protein–PE and PE–PE coacervation, the composition of the condensed phase can be controlled by the mixing ratio (r, protein/PE weight ratio), with the charge imbalance made up by counterions. In a macroion-rich phase with $\rho \neq 1$, excess counterions increase hydration, favoring coacervates relative to precipitates, and for $\rho \gg 1$ or $\ll 1$, destabilizing coacervates with respect to soluble complexes. Soluble complexes, not a separate phase, are free to have non-zero charge, with the compensating counterions subject to dilution. These conclusions are in agreement with experiments that show suppression of coacervation (destabilization with respect to soluble complexes) for β-lactoglobulin–gum arabic[33] and gelatin–gum arabic[34] coacervates with r far from unity. PDADMAC–BSA coacervates prepared in 50 mM NaCl at a fixed bulk stoichiometry corresponding to excess PE charge exhibited values of $\rho < 1$ indicating $[Cl^-] > [Na^+]$ in the coacervate.[1] ρ is thus a complex function of the molecular charges of the two macroions, their structural complementarity, and the ionic strength.

The preceding section is intended to show the points of convergence in the literature on PE–PE coacervation *vis-à-vis* protein–PE coacervation. Turning to protein–PE coacervates, it is important to define these as the macroscopically homogeneous dense phases, not their metastable suspensions, and we then find few reports on their structure, certainly none of which are definitive. This may be because such coacervates have generally been formed from compositionally heterogeneous polyelectrolytes, *e.g.* gum acacia, in combination with inhomogeneous non-globular proteins (*e.g.* gelatin) or globular protein mixtures (*e.g.* whey proteins), leading to large system polydispersity. For this reason, we have focused on the more well-defined coacervates formed from structurally pure globular proteins and structurally homogeneous polyelectrolytes.[1,15,26,35–37] These relatively simple systems still display a set of highly unique properties that suggest complex and fascinating transient patterns of self-organization driven by pure electrostatics.

Rheology and dynamic light scattering (DLS) have been used to examine coacervates formed at different pH and ionic strength (I) conditions from BSA and PDADMAC.[1] Although the system is solid-like at low strain, reconstitution of the elastic behavior after breakage with extensive shear showed the presence of an equilibrium network. Dynamic light scattering studies (DLS) revealed multiple modes of protein diffusion with a fast diffusive mode only an order of magnitude smaller than that of dilute protein, unexpected given the high viscosity. The remarkably robust DLS results obtained from these coacervates requires complete separation of the supernatant phase from the dense coacervate phase by centrifugation. This provides a level of reproducibility, presumably difficult to attain with metastable coacervate suspensions as opposed to equilibrium coacervates. Remarkably, the same three DLS modes are obtained months after an initial run, with only slight diminution of the apparent diffusion coefficients. The slow modes are sensitive to pH and I but insensitive to the molecular weight of the polymer. This behavior showed the importance of electrostatic interactions while also pointing to a structure with a microheterogeneity that allows nearly free diffusion of proteins in certain domains.

Despite these insights into coacervate structure, ref. 1 was inconclusive, finding that experiment could support two very different models. In one, polyelectrolyte networks are crosslinked by one or more proteins with other proteins residing along the non-intersecting PE chains; every protein is assumed to be bound to a PE chain. This ''network model'', is similar to that of Cousin *et al.*[38] proposed on the basis

of SANS measurements, and is a more general form of the one put forward by Huang *et al.*,[39] also based on SANS measurements. In the other "mesophase model", proteins exist in two microdomains, one significantly more concentrated in protein and presumably PE as well. Since available data did not provide an unambiguous conclusion with regard to the two models, other experimental techniques or conceptual approaches are needed to understand the dynamics and structure of coacervates. Probe diffusion offers the advantage of controlling the size of the probe and the degree to which it interacts non-sterically with the matrix being probed.

The exploration of the structure and dynamics of coacervates using probe diffusion can be guided by theories, but attention should be paid to their approximations and limitations. At the most elementary level—probe diffusion in a continuous Newtonian medium—the Stokes–Einstein (S–E) equation is valid; *i.e.* $D = k_B T/6\pi\eta R$, where k_B is the Boltzmann constant, T is the temperature, η the viscosity of the dispersing medium and R the hydrodynamic radius of the probe. A positive deviation from S–E behavior; *i.e.* $D\eta/(D_o\eta_o) > 1$, where D_o is the diffusion coefficient of the probe in the solvent and η_o is the viscosity of the solvent, implies that the probe experiences a local viscosity smaller than the macroscopic or bulk viscosity of the medium. Theoretical models for probe diffusion in polymer solutions and gels, mainly based on obstruction effects, hydrodynamic interactions and free volume effects, have been reviewed by Masaro and Zhu,[40] and Amsden.[41] At a less elementary level, the stretched exponential equation suggested by Phillies[42] fits most of the data in the literature but there is no consensus on the physical meaning of the parameters. Generally speaking the choice of the transport model is highly dependent on the time and length scales of tracer and obstacle mobilities. While normal diffusion models are appropriate for unobstructed diffusion or obstructed diffusion much below the percolation threshold, anomalous diffusion models might be more appropriate for coacervate systems in the time/length scales where behavior is non-ergodic.

In this work we have used fluorescence recovery after photobleaching (FRAP) to study protein diffusivity in BSA–PDADMAC coacervates. In contrast to the mutual or cooperative diffusion coefficients obtained by DLS, those obtained by FRAP closely approximate the self-diffusion coefficients of the fluorescently labeled species.[43] While single particle tracking provides more detail for the diffusion of single or very small groups of particles on distance/time scales of tens of nanometres and tens of milliseconds, respectively,[44] FRAP can probe coacervate structure and dynamics over a wider range of length and time scales. An additional virtue of FRAP is the possibility of varying the probe. Here in addition to fluorescein isothiocyanate (FITC)-labeled BSA (BSA-F), we also use FITC-labeled Ficoll (Ficoll-F), a neutral polysaccharide with a spherical hydrodynamic radius of 4 nm, thus serving as a non-interacting counterpart of BSA. The diffusion of both probes, BSA-F and Ficoll-F, in a neutral medium, namely dextran, was intended to compare diffusivities in coacervates to those in simpler matrixes with identical viscosities, but this approach was vitiated by dextran–protein interactions. FRAP data for Ficoll-F and BSA-F diffusion in coacervates are complemented here by cryo-TEM and static light scattering. These results, in conjunction with DLS data from our previous paper,[1] facilitate the identification of the different motions of both participating and non-interacting tracers at the different length and time scales of coacervates.

Experimental

Materials

Poly(dimethyldiallylammonium chloride) (PDADMAC) was supplied as a commercial sample of "Merquat 100" from Calgon Corporation (Pittsburgh, PA) with a nominal molecular weight of 200 kDa ($M_w/M_n > 10$), dialyzed across a nominal 12–14 kDa molecular weight cut-off membrane (Spectrum, Texas) for two days and freeze-dried prior to use. The PDADMAC sample used for cryo-TEM study was prepared by free radical aqueous polymerization of diallyldimethylammonium chloride, M_n = 144 kDa and M_w = 219 kDa.[45] Regardless of the source of PDADMAC, DLS gave three diffusion coefficients for coacervates,[1] any difference between coacervates made with PDADMAC of broad and narrow M_w distributions attributable to the deconvolution of the autocorrelation function. Fatty acid free bovine serum albumin (BSA) was purchased from Boehringer Mannheim (Indianapolis, IN) as 99% pure lyophilized protein, although BSA used in FRAP spot bleaching experiments was obtained from Sigma Chemicals (gel electrophoresis grade with nominal purity between 96 to 99%). Identical results obtained with BSA from the two different sources, as mentioned below, indicate the sufficiency of the protein level of purity. Fluorescein isothiocyanate (FITC) was obtained from Sigma (F4274, Lot#: L2506). Ficoll fraction 7 (Ficoll-7) was a gift from Dr Rune Andersson of Pharmacia Biotech AB (Sweden) with M_w = 37 kDa, M_w/M_n = 1.18, R_s = 3.8 nm. Dextran (T-500) was from Pharmacia Biotech AB (Sweden) with a nominal weight average molecular weight of M_w = 509 kDa and M_w/M_n = 2.9. Sephadex G-25 (27106-3) was purchased from Aldrich. Whatman cellulose acetate disposable filters were used for sample clarification. All experiments were conducted at room temperature (25 $\pm$ 3 °C). FITC labeled BSA (BSA-F) and Ficoll (Ficoll-F) were prepared by Wang[37] using a modification of the labeling methods of Crandall *et al.*[46] and Luby-Phelps,[47] respectively, and purified by chromatography on Sephadex G-25. BSA-F and Ficoll-F labeling for spot bleaching FRAP samples was done by Dr Lawrence Mark[48] by following the methods of Millett *et al.*[49] and Luby-Phelps,[47] respectively. The number of FITC groups per BSA is 2 $\pm$ 0.5 while the number of FITC groups per Ficoll is 0.2.

Methods

Sample preparation. BSA-F or Ficoll-F were incorporated into the dextran solutions of 20, 30, 35, 40% (by weight) in 0.05 and 0.1 M NaCl by overnight mixing of the probe solution with the polymer solution. The BSA-F and Ficoll-F concentrations in dextran were 0.025 g L^{-1} and 0.25 g L^{-1},

respectively, and pH was adjusted by addition of 0.1 N HCl or 0.1 N NaOH.

For FRAP in coacervates, BSA was directly dissolved at 4 g L^{-1} in de-ionized water adjusted to the required ionic strength and doped with 0.04 g L^{-1} BSA-F. The polymer solution (0.8 g L^{-1}) was prepared similarly. These stock solutions were filtered (0.45 μm), titrated to pH = 4, and then mixed to give a protein-to-polymer weight ratio r = 5. After stirring for 4 h, the mixture was titrated with 0.1 M NaOH to the desired pH, to yield mixtures with ionic strengths (I) 0.05 to 0.1 M NaCl at pH 7.5, 8.5, and 9.5. The turbid preparations thus obtained were centrifuged at 4000 rpm for several hours until a clear supernatant could be separated from the clear and more dense coacervate phase. This was loaded into 5 ml cylindrical quartz cells and centrifuged for one hour. Supernatants were removed from coacervates with a disposable pipette. A tissue was then used to soak up any residual supernatant. Samples used for static light scattering and cryo-TEM were also prepared as above but without addition of FITC labeled probes.

A more facile method of sample preparation was found to give equivalent results and was employed for stripe bleaching experiments. BSA-F and Ficoll-F probes were incorporated into the coacervates by dissolving the probe in the supernatant (dilution ratio of 1 : 5000), and then agitating 1.5 g ($\sim$1.5 ml) of pure coacervate with 0.5 ml of supernatant. After centrifugation, residual supernatant was removed from the coacervates by wicking with a tissue.

Fluorescence recovery after photobleaching (FRAP). Initially, FRAP data were obtained by spot bleaching. Subsequently, more detailed experiments were done by stripe bleaching. Several experiments were done in duplicate conditions to show that average diffusivities obtained by the two methods are interchangeable. For example, the diffusion coefficients of BSA-F in a BSA–PDADMAC coacervate of pH = 8.5 and I = 0.1 M NaCl were 0.46 $\times$ 10^{-7} and 0.41 $\times$ 10^{-7} cm^2 s^{-1} for spot and stripe bleaching, respectively. Fast and slow FRAP modes were reported only based on stripe bleaching experiments. Regardless of the methodology and the nature of the probe, probe concentration was always small enough (*e.g.* 1/1000 of coacervate protein concentration) to ensure the absence of perturbation of coacervate structure.

i) Spot bleaching. Spot photobleaching was carried out in the laboratory of V. Bloomfield (University of Minnesota).[50] The instrument comprised a 200 mW, water cooled argon ion laser (model 95-3, Lexel Corp., Fremont, CA) operated at 488 nm and the signal was detected at photon-counting mode. Coacervates prepared as described above were placed onto flat microslides (path-length 0.2 mm) within a ring of vacuum grease and then covered with a coverslip. In order to prevent binding of labeled BSA to the glass walls, the slides were passivated by rinsing with unlabeled BSA solution, followed by vacuum drying at room temperature. Sample preparation was done as described above. After 500 ms bleaching time, the recovery of fluorescence through diffusion of bleached and unbleached BSA-F was recorded as a function of time. Assuming a Gaussian intensity profile for the laser beam, the fluorescence recovery $F(t)$ is given by

$$F(t) = F_\infty \exp\left[-\frac{2}{1+(8tD/a^2)}\right] \quad (1)$$

where F_∞ is the intensity at full recovery, and a and D are spot size (50 μm for our experiments) and probe translational diffusion coefficient, respectively.[51,52] Full recovery was observed in 2–3 minutes for dilute solutions of BSA-F and Ficoll-F but only 75–80% recovery was obtained after 30 min for coacervate. All spot bleaching data could be least-squares fitted to eqn (1) with correlation coefficient better than 0.97.

ii) Stripe photobleaching with modulation. The details for FRAP stripe bleaching are given elsewhere.[53] Briefly, an electromechanical modulation detector system was used to monitor the AC amplitude, which was either fit to a single exponential (eqn (2)) or a double exponential decay expression (eqn (3))

$$C_1(t) = A_o\exp(-K^2D_st) \quad (2)$$

$$C_2(t) = A_1\exp(-K^2D_1t) + A_2\exp(-K^2D_2t) \quad (3)$$

where A_i is the AC amplitude at the baselines of the fit, D_s is the self-diffusion coefficient of the fluorescent labeled molecules, $K = 2\pi/L$ is the spatial frequency, and L is the distance between stripes of a translated grating pattern (Ronchi ruling).[54] Fitting with more than two diffusion coefficient modes yielded a third mode smaller than 5% whose existence was thus highly questionable. During the experiment, selected samples were measured at different K values to ensure the absence of the nondiffusive fluorescence recovery. For most of the experiments, we used a Ronchi ruling with L = 100 and an objective magnification of 10×, corresponding to K = 778 cm^{-1}. One of the major advantages of stripe bleaching is the shallow bleach depth, avoiding the problem of partial recoveries usually observed in spot photobleaching instruments.

Static light scattering (SLS). Static light scattering (SLS) experiments were performed on BSA–PDADMAC coacervates prepared at r = 5, pH = 9.0 and ionic strengths 10, 20, 50 and 100 mM using a BI-200 SM goniometer and BIC-2030D (Brookhaven Instruments Inc.) photon counting system with an Omnichrome Ar-ion 100 mW laser (wavelength = 488 nm) as excitation source. The intensity of the light was measured as a function of angle for 10 scattering angles chosen between 30° and 120°. The samples were prepared as in the coacervate preparation section but without fluorescent labeled probes. The data were fitted to the Guinier relation: $I(q) = I_o\exp(-q^2R_g^2/3)$. R_g, the radius of gyration, is determined from the slope of ln $[I(q)]$ *vs.* q^2.

Viscosity measurements. Rheological data were obtained at Osaka University by T. Shikata and A. Hashidzume using a DynAlyser 100 stress-control rheometer (RHEOLOGICA,

Sweden) equipped with a cone and plate at 25 °C. The radius of the cone was 40 mm, and the angle between the cone and plate was 4.0°. Macroviscosities (zero-shear viscosities) η were obtained from

$$\eta = \lim_{\omega \to 0} (G''/\omega) \quad (4)$$

where ω is the angular frequency, and G'' is the loss modulus at ω.[55] These results were supplemented by data from ref. 1.

Cryogenic transmission electron microscopy (cryo-TEM). Cryo-TEM was performed on BSA–PDADMAC coacervate prepared at r = 5, pH = 9.0 and I = 50 mM NaCl. Sample preparation, transfer and imaging are done following the same procedure described before for mixtures of micelles with phenolic organic dopants.[56] All sample preparation was done in a controlled environment chamber, where the temperature and solvent partial pressure are controlled carefully to maintain the sample temperature and suppress any evaporation. A drop containing a few microlitres of the fluid sample, equilibrated within the chamber, is withdrawn using a pipette and deposited onto a specially prepared holey carbon grid. The drop is blotted, leaving behind thin films of liquid (thickness from 50–200 nm) spanning the holes. The sample is then plunged into a cryogen reservoir, typically liquid ethane close to its melting point. Contact with the cryogen induces rapid solidification of the sample, causing the water in the solution to vitrify rather than crystallize. *This rapid vitrification preserves all of the microstructures in their original state*. The microscope grid is then transferred under positive dry nitrogen pressure to a cold stage (Oxford Instruments CT3500J), and maintained at ~ -165 °C during phase contrast imaging in the electron microscope. The low sample temperature prevents the amorphous–crystalline transformation in the vitrified sample, suppresses sublimation and minimizes beam damage.

Results and discussion

BSA and Ficoll in dextran

Interpretation of the FRAP results for BSA-F in coacervate must take into account that this probe interacts with the matrix both sterically and enthalpically. To resolve structural effects from interaction effects, four comparisons were considered: (1) BSA in dextran *vs.* BSA in coacervates, (2) BSA in dextran *vs.* Ficoll in dextran, (3) Ficoll in dextran *vs.* Ficoll in coacervates, and (4) Ficoll in coacervates *vs.* BSA in coacervates. As will be explained, (1) and (2) were impeded by BSA–dextran interactions. We mention (3) for general interests, although largely outside the scope of this paper. The fourth comparison will be directly relevant to our main purpose of determining structure and dynamics in coacervates.

Initially, we chose dextran as a reference matrix, specifically with the intention to compare the diffusion of BSA in a coacervate with its diffusion in a dextran solution that has the same macroviscosity. Such a comparison would be based on the assumption that the interactions of BSA with dextran are purely steric. This was tested by comparison of BSA–dextran with Ficoll–dextran, the latter being an ideal

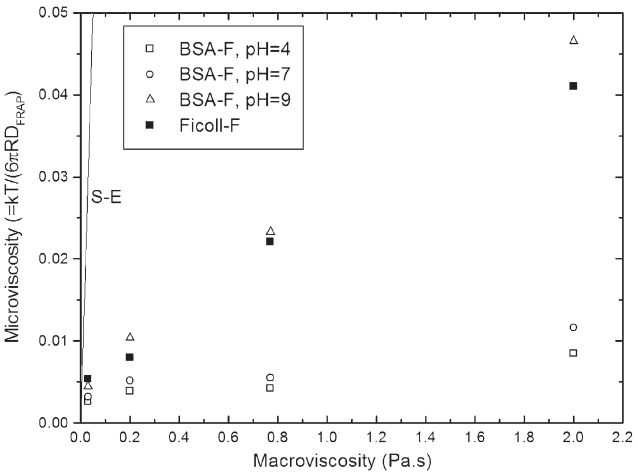

Fig. 1 BSA-F and Ficoll-F diffusion in dextran. The salt concentration was 0.1 M NaCl in all samples. The Stokes–Einstein relationship is shown with the solid line. □: BSA-F at pH = 4, ○: BSA-F at pH = 7, Δ: BSA-F at pH = 9, and ■: Ficoll-F at pH = 5.5.

non-interacting pair. We report these results in Fig. 1 as the relationship between macroviscosity and "microviscosity" $\eta D = kT6\pi/RD_{\mathrm{FRAP}}$, *i.e.* the viscosity calculated from the diffusion coefficient using the Stokes–Einstein (S–E) expression along with the radius and diffusion coefficient of the probe molecule (Ficoll-F or BSA-F). This plot is the inverse of the dependence of measured diffusivity on bulk viscosity; it allows for graphical display of deviations from S–E behavior, the solid line in Fig. 1. Apparently, dextran solutions do not constitute a continuum, a result consistent with other studies of probe diffusion in polymer solutions:[52,57–60] the large deviations from S–E behavior mean that even an inert probe such as Ficoll experiences regions of high and low dextran concentration during its motion. The deviations from S–E behavior in Fig. 1 include Ficoll–dextran behavior to illustrate how departures in the direction of low slopes demonstrate progressive matrix heterogeneity. The results for BSA-F at pH 9.0 are very similar to Ficoll-F, but BSA-F at lower pH deviates strongly from the behavior of Ficoll-F, even though their diffusivities in water are nearly identical. The pH-dependence of the BSA-F results and their deviation from Ficoll-F suggests interactions between BSA-F and the matrix. Consistent with this is the finding of an interaction between dextran and BSA, strong enough to lead to partial protein unfolding under some conditions.[61] While the nature of the pH effect and how it leads to higher diffusivity for BSA than Ficoll at pH 4 and 7 is not understood, such interactions severely compromise the use of BSA–dextran as a reference system and limit the use of dextran as a reference matrix.

BSA-F and Ficoll-F in coacervates: general remarks

Fig. 2 shows the relationship between microviscosity η_{D} and macroviscosity η for BSA and Ficoll in coacervates, and for Ficoll in dextran. While the macroviscosities of dextran are controlled by the dextran concentration, those of the coacervates are controlled by the pH and ionic strength. We begin with the somewhat surprising result that Ficoll-F

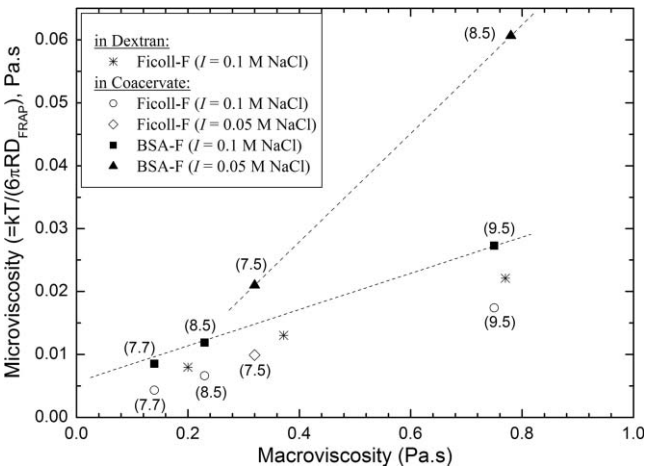

Fig. 2 Comparison of diffusivities in dextran and in coacervates. Ficoll-F and BSA-F diffusivities are from single exponential fit of the data. pH values of coacervate preparation are shown in parentheses. *Ficoll-F in dextran (I = 0.1 M NaCl), ○: Ficoll-F in coacervate (I = 0.1 M NaCl), ◇: Ficoll-F in coacervate (I = 0.05 M NaCl), ■: BSA-F in coacervate (I = 0.1 M NaCl); ▲: BSA-F in coacervate (I = 0.05 M NaCl). The lines are drawn to guide the eye.

diffuses more rapidly in coacervates than in dextran of the same η. Since Ficoll-F is a passive observer of both matrixes, this provides an indication of the difference between the structures of coacervates and of systems of entangled chains. There are two perspectives for interpretation: (1) partially interconnected (non-isolated) regions of low effective viscosity in the coacervates allow for rapid motion of Ficoll-F relative to an entangled dextran network of the same η; and (2) at equal values of Ficoll-F diffusivity, there are structural features in the coacervates that lead to an "anomalously high" η, an effect not seen by an inert diffusing probe. The choice of axes in Fig. 2 indicates our intention to use the first approach, *i.e.* η as the independent variable.

As a passive observer, Ficoll-F can probe the structure of the BSA–PDADMAC coacervates more objectively than BSA-F, which is an active participant. Put differently, while FRAP with Ficoll-F should provide information about the structure and dynamics of the coacervates, results with BSA-F also reflect this probe's electrostatic interactions at and within the various domains that may exist. Such domains were implicit in the preceding remark on regions of low effective viscosity, implying as well regions of high viscosity (also inferred from prior DLS and rheology studies).[1] To some extent, these domains result in obstructed diffusion. We consider first in detail the results for Ficoll-F as a non-interacting probe of these proposed obstacles.

Ficoll-F in coacervates

Spatial heterogeneity. While the data presented in Fig. 2 are based on average diffusivities from FRAP, all measurements for Ficoll-F in coacervates were clearly resolved into fast and slow exponential decays, as shown in Table 1. The presence of resolvable fast and slow diffusion coefficients for the neutral probe indicates heterogeneities in the coacervate. Evidence in support of such microheterogeneities comes from several sources. Detailed analysis of DLS for the same protein–polyelectrolyte coacervate systems[1] revealed two or three diffusional modes depending on the pH and ionic strength of the coacervate. The dominant DLS scattering arose from a fast mode with diffusivities $D_{\mathrm{fast}}^{\mathrm{DLS}}$(BSA), only five times smaller than in free solution: $1.5 \pm 0.3 \times 10^{-7}$ *vs.* 7×10^{-7} cm^2 s^{-1}, respectively. A second DLS diffusive mode $D_{\mathrm{S1}}^{\mathrm{DLS}}$(BSA) indicated motions an order of magnitude slower than the fast mode. Coacervates prepared under conditions of strong protein–PE electrostatic interaction (pH $\geqslant$ 8.5 and $I \leqslant$ 50 mM) displayed an additional nondiffusive (angle-dependent) slow mode ("S2" in ref. 1). The first two modes were attributed to BSA diffusion in, respectively, dilute and dense domains. While that work offered no direct information on the size of the dense domains, rheology suggested that they were large enough to form "solid-like tenuous microdomains/networks embedded in a viscous fluid subject to disruption by shear".[1] Viscoelasticity measurements of coacervates showed an increase in shear modulus with protein–polyelectrolyte electrostatic interactions, arising from connectivity of these proposed microdomains.

The probable size of coacervate dense domains can be estimated from light scattering data and imaging results. Fig. 3 presents the former for samples prepared at pH = 9.0 and in salt concentrations ranging from 10–100 mM. Guinier plots were used to obtain average radii of gyration of the strongly scattering objects, leading to R_g = 137 $\pm$ 7 nm, invariant with ionic strength. While this dimension is close to the Guinier limit of qR_g = 1, it is consistent with the cryo-TEM image of Fig. 4 for a BSA–PDADMAC coacervate prepared at pH = 9.0 and I = 50 mM NaCl, in which protein-rich microdomains appear as dark regions with blind alleys along

Table 1 FRAP and DLS[1] diffusion coefficients

			DLS (BSA)/ $\times 10^7$ cm^2 s^{-1}			FRAP			
						BSA/ $\times 10^7$ cm^2 s^{-1}	Ficoll/ $\times 10^7$ cm^2 s^{-1}		
pH	I/mM	Viscosity/Pa s	Fast	S1	S2	Average	Average	Fast	Slow
9.5	100	0.75	1.55	0.14	—[b]	0.18	0.33	0.7	0.2
8.5	100	0.23	1.7	0.13	—[b]	0.46	0.87	1.5	0.63
7.7	100	0.14[a]	—	—	—	0.64	1.33	1.8	0.55
9.0	50	1.3	1.2	0.03	0.004	—	—	—	—
8.5	50	0.78	1.3	0.08	0.018	0.09	—	—	—
7.5	50	0.32	0.9	0.07	—[b]	0.26	0.58	1.7	0.55

[a] Viscosity obtained at pH = 7.6 and I = 0.1 M NaCl. [b] No S2 was observed at this condition.

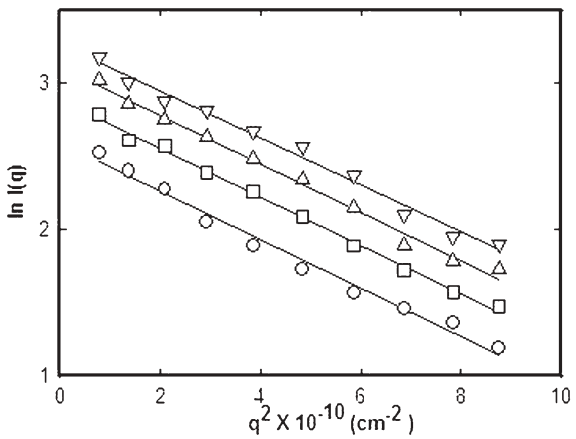

Fig. 3 Guinier plots from SLS for coacervates prepared at $r = 5$ and pH = 9.0; 10 mM (open circle); 20 mM (open square); 50 mM (open triangle) and 100 mM (inverted open triangle) NaCl.

the dilute domain (light regions) interface. Structures of this sort were previously inferred from rheology data, *i.e.* G' above G'' at low frequency and the slow recovery of G' after preshearing both suggesting a tenuous network of solid-like objects. The appearance of non-diffusive slow modes in DLS will be correlated (below) with the forming and reforming of such structures in the absence of shear. Naturally such three-dimensional structures can only be visualized in two dimensions by cryo-TEM. Taken together, these two results strongly suggest a coacervate structure of protein-rich domains with typical interdomain distances of 300–700 nm, and they provide a working hypothesis for the interpretation of FRAP data: coacervate structures consist of partially interconnected clusters (also called "dense domains"), the lifetimes of which are correlated with their size. Analysis of FRAP data can then be used to refine or refute this model.

Table 1 shows that values for $D_{\mathrm{fast}}^{\mathrm{FRAP}}$(Ficoll) and $D_{\mathrm{fast}}^{\mathrm{DLS}}$(BSA) are very similar, 0.7–1.8 and 0.9–1.7 $\times$ 10^7 cm^2 s^{-1}, respectively. This is a surprising result for two reasons. First, diffusivities measured by FRAP are frequently smaller than diffusivities by DLS because of the different length scales.[60] The characteristic length scale for stripe bleaching FRAP here is $2\pi/K = 80$ μm, where K depends on the number of stripes per unit length and the magnification of the objective. This is approximately three orders of magnitude larger than that length scale of DLS, $2\pi/q = 250$ nm, where q is the scattering wavevector $q = 4\pi n(\sin(\theta/2))/\lambda$. (The time scale for stripe bleaching experiments, *i.e.* the longest time for the fluorescence intensity decay curve to reach an asymptote, was 2–8 minutes, while the time scale for DLS, *i.e.* the asymptotic time for the autocorrelation function, was 2–200 ms.) At the long length scale of FRAP, obstacles (dense domains) can slow down diffusion, while obstacles become unimportant at the length scales of DLS and the probes take a direct, continuous path. Second, the interaction of BSA with the matrix should impede its diffusion compared to Ficoll. These two effects must be considered before concluding that the result $D_{\mathrm{fast}}^{\mathrm{FRAP}}$ (Ficoll) $\approx$ $D_{\mathrm{fast}}^{\mathrm{DLS}}$ (BSA) arises from their fortuitous cancellation.

In order to interpret the similarity of the fast diffusion coefficients for Ficoll (from FRAP) and for BSA (from DLS)

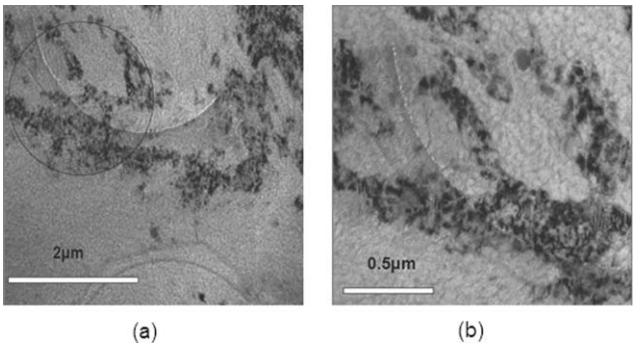

Fig. 4 BSA–PDADMAC coacervate prepared at pH = 9.0, I = 50 mM NaCl; (b) is a zoomed-in version of the circled region in (a).

we need to consider both the morphology of the dilute domain and its ability to interact with these two solutes. The volume fraction of the dilute mesophase estimated from the cryo-TEM image (Fig. 4), $\Phi_{\mathrm{dilute}} \approx 0.85$, is consistent with the fact that 75% of DLS scattering comes from proteins in this dilute domain, its volume fraction then >75%. Both results suggest that dense domains are far from percolation, so that both Ficoll and BSA can move through dilute domains without substantial perturbation from dense clusters. With regard to interactions with the dilute domain matrix, the replacement of dilute domain bleached Ficoll-F with unbleached probes in FRAP involves the same hopping motion used by BSA to travel in the dilute mesophase in DLS. These displacements are facilitated by the continuous and very rapid fluctuations of PE segment densities in the coacervate, calculated elsewhere with a relaxation time on the order of 0.01 ms.[62] In summary, the similarity of diffusion coefficients for the BSA (DLS) and Ficoll (FRAP) fast modes is explained by the unobstructed free diffusion in the large volume fraction of the dilute mesophase for BSA-F and Ficoll-F, facilitated by polymer segment density fluctuations.

In contrast to fast mode diffusion coefficients, Ficoll-F slow mode diffusivities ($D_{\mathrm{slow}}^{\mathrm{FRAP}}$(Ficoll)) are larger than the values for BSA slow mode 1 ($D_{\mathrm{S1}}^{\mathrm{DLS}}$(BSA)). Recovery from bleaching in the dense domains involves the release of bleached Ficoll by dissolution of dense clusters on time scales anywhere from tens of ms, obtained from the non-diffusive (angle-dependent) DLS "slow mode 2",[1] to hundreds of seconds (as obtained from the recovery time of the elastic modulus after pre-shearing),[1] depending on cluster size. The diffusive (angle-independent) DLS modes with relaxation times $\leqslant$1–5 ms fail to capture dense domain dissolution effects, in contrast to the FRAP slow mode which combines diffusion inside the dense clusters and facilitated diffusion due to their breakup.

Interactions affect structure. Rheology and DLS reported elsewhere[1] clearly demonstrate the response of coacervate structure to BSA–PDADMAC electrostatic interactions, enhanced by an increase in pH or a decrease in ionic strength I during coacervate preparation. It was therefore expected that diffusion coefficients for Ficoll-F in coacervates should depend on these variables. As shown in Fig. 5, the average values for $D_{\mathrm{avg}}^{\mathrm{FRAP}}$(Ficoll) as a function of macroviscosity are consistently smaller at I = 50 mM than at I = 100 mM at all pH's. On the

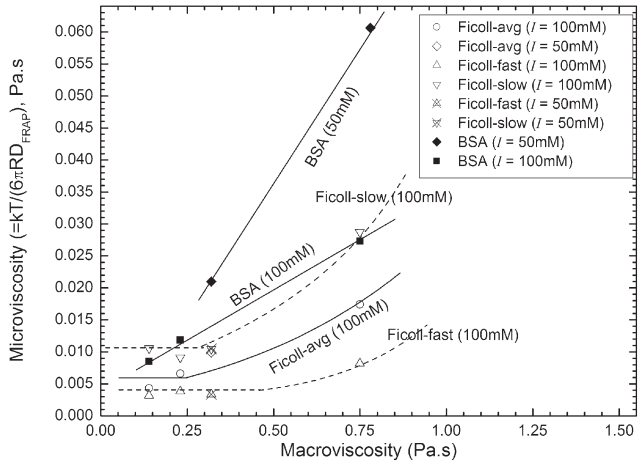

Fig. 5 Microviscosity *vs.* macroviscosity for Ficoll-F and BSA-F in coacervates. Ficoll-F average and BSA-F data were previously presented in Fig. 2. The lines are drawn to guide the eye.

other hand, DLS suggests that the volume fractions of dense domains are not salt-dependent, since the scattering intensities for slow modes account for 15% of the total scattering regardless of *I*. Thus, the larger D_{avg}^{FRAP}(Ficoll) at higher salt concentration is not due to reduction in the volume fraction of dense domains but could be related to changes in their size or number density. An examination of such effects leading to a relationship between structure and dynamics, can be based on theories for probe diffusion in porous/multichannel liquid mediums.[63–65] Since these theories are valid only for stationary obstacles, we will first determine whether our obstacles (dense domains) look "immobile" for a probe diffusing in the dilute domain.

To evaluate obstacle lifetime relative to probe diffusion, we first attempt to estimate the probe diffusion rate within the cavities (or "blind alleys") of the dense domains *vs.* the rates of obstacle dissolution/disintegration. The relevant parameter is the time t_x it takes the probe to escape from such an enclosure relative to its lifetime. The obstacle disintegration times (the obstacle lifetimes) were identified with the non-diffusive DLS relaxation times (τ_{S2}) obtained from the angle-dependent[1] slowest DLS modes (S2). This identification is supported by the much larger DLS relaxation time τ_{S2} compared to τ_{S1} or τ_F. The obstacle disintegration time τ_{S2} can be then compared with the backtracking time t_x:

$$t_x = \frac{\langle r^2 \rangle}{6D} \quad (5)$$

where $<r^2>$ is the trajectory path-length, and *D* is the diffusion constant of the probe in dilute domain, taken from the DLS fast mode for BSA. Fig. 4 represents a two-dimensional slice of one of many three-dimensional obstacles in one particular sample. Invocation of eqn (5) involves the assumption of unconfined diffusion, strictly correct only when the probe is small relative to the dimensions of the enclosure, the cryo-TEM image suggesting enclosure dimensions an order of magnitude larger than the probe. Since our purpose is only to evaluate the premise that such obstacles persist over the lifetime of enclosure, we use 500 nm for the corresponding path-length to estimate typical values for $<r^2>$ leading to the values of t_x in Table 2. The observation that $\tau_{S2} > 3t_x$ indicates that obstacles (dense domains) are stationary within the time scale of probe captivity.

Table 2 Relaxation (recovery) times from DLS and probe back-tracking time

pH	*I*/mM	M_w/kDa	t_x[a]/ms	τ_{S2}/ms	τ_{S1}/ms	τ_F/ms
8.5	100	~200/219	2.5	—[b]	1.5	0.09
9.5	100	~200	2.7	—[b]	1.3	0.11
7.5	50	219	4.6	—[b]	2.36	0.18
8.5	50	219	3.2	8.85	2.2	0.176
9.0	50	219	3.5	30.8	3.5	0.15

[a] t_x: backtracking time (refer to eqn (5) and the relevant text for more detailed explanation). [b] No S2 mode was observed.

Having concluded that dense domains can behave as quasi-stable obstacles, we can discuss the drop in FRAP diffusivities upon decrease in *I*, using theories for probe diffusion in a porous/multichannel liquid. These theories can be formulated as:[63–65]

$$D_{eff} = D_o(P/T)H \quad (6)$$

D_o is the unhindered probe diffusion coefficient which we will take as the diffusion coefficient of either probe in the dilute domain, *i.e.* $D_o = D_{fast}^{FRAP}$(Ficoll) $\approx D_{fast}^{DLS}$(BSA) = 1.45 × 10^{-7} cm^2 s^{-1}. The porosity $0 < P < 1$, is the obstacle-free cross-sectional area fraction, estimated from Fig. 4 as $P \approx 0.85$, and considered constant at all salt and pH conditions. The hindrance factor, $0 < H < 1$, a function of the ratio of the probe diameter to the mean channel width, is taken here as unity since the tracer size is much smaller than the channel width. The tortuosity, $1 < T < \infty$, is the ratio of the mean path through the medium to the corresponding linear distance. With *P* and *H* fixed, we see that increased tortuosity alone could lead to a reduction in *D*. This high tortuosity could arise under conditions of stronger electrostatic interaction from either an increase in the interconnectedness of dense domains or an increase in their lifetime, *i.e.* low *T* could correspond to either more isolated or more transient dense domains. In DLS, decrease in *I* from 100 to 50 mM NaCl at pH = 8.5 leads to the appearance of S2, the non-diffusive second slow mode,[1] suggesting more durable obstacles. Since fast modes correspond to free diffusion within channels, no effect appears and there is no effect of *I*. In summary, the diminution of D_{avg}^{FRAP}(Ficoll) with decreased *I* is attributed to the stabilization of clusters which function as less transient obstacles.

We now consider the influence of pH on Ficoll-F diffusion at constant *I* (100 mM). As seen in Fig. 5, these diffusivities stay relatively constant at low pH and macroviscosities until pH 9.5, at which point the rapid upturn corresponds to a marked decrease in diffusion rates. This condition of high pH corresponds to strong protein–PE interaction as manifested in *e.g.* large increases in viscosity, a five-fold increase in shear modulus, and the appearance of non-diffusive slow modes in DLS,[1] all of which attest to an increase in the interconnectivity and lifetimes of the dense domains. This suggests the presence of more stable and interconnected obstacles that do not break up during the time frame of probe diffusion (see Fig. 6 for a

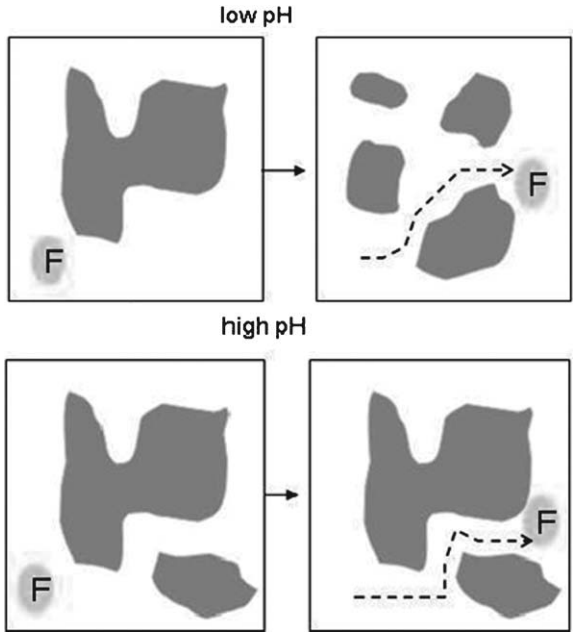

Fig. 6 Schematic description of probe path at low and high pH.

sketch). The constancy of the fraction of light scattered from dilute domains with respect to pH[1] indicates that the volume fraction of dense domains is rather constant, so only their connectivity and durability change with pH. Thus the marked decrease in Ficoll FRAP diffusivities at high pH could be due to anomalous diffusion within the blind alleys of the interconnected obstacles suggested by the cryo-TEM image of Fig. 4.

BSA-F in coacervates

The inert probe Ficoll-F explores the obstruction of fast diffusion in the dilute domain by dense domain obstacles, visualized as quasi-immobile objects with cavities whose effect can be reduced by disintegration. The charged probe BSA-F is in addition influenced by interactions at dense/dilute domain interfaces (adsorption), while both are subject to the effect of entrapment within dense domains. By way of analogy, Verkman[66] compared diffusion in cytoplasm to road travel, with the transit time depending on: (a) the mean velocity during motion (here taken as the fast diffusivity), (b) the stoplights (here, adsorption at interfaces), and (c) the route (obstructions, here changeable due to their disintegration). For the coacervates, pH and ionic strength apparently have little influence on (a), but the other effects may not be fully resolved.

While the fast mode for Ficoll-F may be ascribed to velocity (a), well-resolved from adsorption and embedding, the inability to resolve fast and slow components for BSA-F points to intermediate recovery modes, related to adsorption at interfaces absent for Ficoll-F. The replacement of bleached embedded BSA-F with unbleached protein involves both diffusion within and disintegration of dense domains. Due to electrostatic forces, BSA-F diffusion is slowed down as pH is increased or I is decreased (see Table 1, Fig. 2 or 5). Such a direct correlation between D and electrostatic interaction strength for Ficoll-F is only observed when pH is increased to 9.0 in 100 mM NaCl, presumably due to longevity of obstacles. The fast and slow modes of diffusion for BSA-F can be separated by DLS, and it is tempting now to assign the slower DLS diffusive mode relaxation (“S1”) to adsorption, and the very slow non-diffusive mode “S2” to dense domain disintegration.

Molecular models

The present results can be considered in the context of the models previously advanced for the structure of polyelectrolyte–protein coacervates; *i.e.* the mesophase model and the network model. The two resolvable fluorescence recovery modes for Ficoll-F reported here strongly suggest the presence of phases of low and high effective viscosities. These observations are entirely consistent with DLS results[1] including quantitative agreement of fast mode diffusivities, despite the difference in length scales between FRAP and DLS. The limited SLS and cryo-TEM results reported here in Fig. 3 and 4 are also consistent with dense (protein-rich) phases, with irregular geometries but typical length scales of a few hundred nm. Weak, very fast DLS modes[62] along with previous SANS data[67] both indicated (model-dependent) polyelectrolyte mesh size on the order of ξ = 2–3 nm. This value of ξ, consistent with the calculated polymer segment density, is smaller than the protein radius, which does not support models[38,39] in which proteins are crosslinks. In summary, while SANS appears to support the network model, FRAP, DLS and cryo-TEM are in better agreement with the mesophase model, with rheology being inconclusive on this question.

A fundamental difference between the two models is the extent to which the short-range structure of soluble polyelectrolyte–protein complexes is retained in coacervates, *i.e.* whether proteins “belong” (at least transiently) to particular polymer chains. In our current understanding of the mesophase model, the polymer segment density is too large to justify this point of view as the electrostatic potential landscape of a 4 wt% polyelectrolyte solution (*i.e.* its concentration in coacervates)[1] is virtually continuous on the protein length scale, albeit with rapid local fluctuations. Furthermore, if protein motion were strongly coupled to the motions of polymer chains to which they were specifically attached, Ficoll molecules, free of such constraints, would move more rapidly than protein, whereas we observe nearly identical values for $D_{\mathrm{fast}}^{\mathrm{FRAP}}$(Ficoll-F) and $D_{\mathrm{fast}}^{\mathrm{DLS}}$(BSA). Thus, proteins are not fixed in position, but interchange readily with concomitant polyelectrolyte fluctuations, which provide little effective friction in the dilute domains. The consequence of intensified protein–polyelectrolyte interactions, *via* increase in pH or reduction in ionic strength, is certainly clear from rheology, but a remarkable feature is the lack of diminution of fast diffusional modes from either DLS (BSA) or FRAP (Ficoll-F) upon decrease in I at constant pH, or upon increase in pH and constant I. All of these effects show that diffusive motions in the dilute domain are unrestricted either sterically or enthalpically.

We next consider non-enthalpic contributions to coacervate stability. In common with the phase separation of oppositely charged polyelectrolytes,[2,32] the driving force for coacervation

should be charge neutralization and counterion release. If the entropy gain for the latter is dominant, coacervation need not be exenthalpic. Consistent with this is the fact that pH_ϕ shows no temperature dependence,[27] and that mixing of BSA and PDADMAC by isothermal titration calorimetry at conditions of coacervation yields no heat.[68] On the other hand, complexation of β-lactoglobulin with pectin[69] or chitosan[70] is exenthalpic. The relative contributions of entropy and enthalpy for protein–polyelectrolyte complexation may be highly system-dependent as is the case for interpolyelectrolyte complexation,[71] but counterion release can be expected to contribute favorably in both cases, as well as in mesophase segregation, where the overall entropy reflects a delicate balance of the favorable effect of counterion release and the unfavorable restrictions on polymer configuration. Our description of coacervation must include not only the driving force for mesophase segregation but also some understanding of its length scale.

We proceed by considering the manner in which coacervates are built up, recognizing that some of the steps may be hypothetical as opposed to kinetically meaningful. For both protein–polyelectrolyte and micelle–polyelectrolyte systems, soluble complexes and their higher-order (but still soluble) aggregates achieve electrophoretic neutrality as a precondition of coacervation.[72,73] However, experiments with micelle–polyelectrolyte systems in particular[6] show that the range under which coacervates form is broader than the exact point of electrophoretic neutrality. This indicates that neither intrapolymer soluble complexes nor their higher-order aggregates are stoichiometric:

$$Z_P \neq nZ_{pr} \text{ or } \alpha Z_P \neq \alpha n Z_{pr} \quad (7)$$

where Z_P and Z_{pr} are the net charge on polyelectrolyte and protein, respectively; n is the average number of proteins bound per polymer chain, and $\alpha \geqslant 1$ is the degree of aggregation. To some extent small ions can compensate this charge imbalance but evidently not to the extent to produce zero mobility at the point of incipient coacervation.[72,74]

The electrostatic energy of a protein transiently at the periphery of a soluble complex is larger than one less distal because it is removed from the center of mass of polyelectrolyte segments; this form of surface energy promotes coalescence, providing an enthalpic driving force for aggregation which is accompanied by the favorable entropy of the release of counterions. This process is kinetically driven by a form of polarization, in which the protein-rich (net negative) region of one complex can induce and interact with the polyelectrolyte-rich (positive) domain of another. At this point entangled polyelectrolyte chains begin to present a more or less homogeneous electrostatic environment to the embedded proteins. Unlimited continuation of this clustering process would lead to the separation of a second phase (coacervates), but not necessarily one that is itself mesophasic.

However, since soluble complexes and their aggregates need not be electrically neutral, charge accumulates as they coalesce into a phase containing clusters of aggregates. Something like this ''Coulomb-blocked aggregation'' has been described by Meyer *et al.*[75] for negatively charged Ag colloids, which leads to finite size of clusters. In other words, clusters are size-limited to the extent that the interfacial force cannot compensate for the longer-range repulsions. In the present case, the formation of domains dense in both proteins and polyelectrolytes goes hand-in-hand with counterion expulsion, due both to Donnan effects and to the diminished ability of protein and polyelectrolyte to suppress counterion activity coefficients (*i.e.* liberation of ''bound'' counterions''). Clusters thus not only have net charge, but also diminished ionic strength relative to bulk coacervate values. The relatively lower salt concentration and higher polyelectrolyte segment concentration in the dense phase are all in agreement with the recent model of Allen and Warren for polyelectrolyte–surfactant complexation.[76] Counterion release into dilute (unclustered) domains contains an entropically favorable term, and also enables these dilute domains to screen repulsive interactions among clusters.

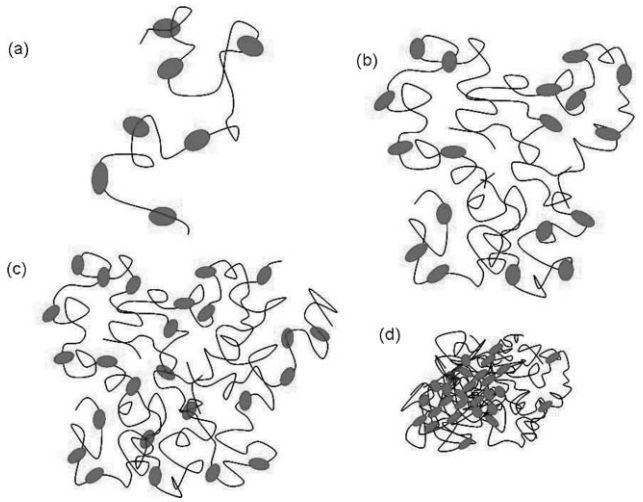

Fig. 7 Coacervate formation. (a) Intrapolymer complex, (b) soluble aggregate of (four) intrapolymer complexes, (c) hypothetical intermediate interpolymer complex, (d) coacervate with dense and dilute domains. (Length scale: protein diameter (ellipses) = 8 nm.)

In Fig. 7(b), soluble aggregates are represented by assemblies of intrapolymer complexes whose favorable overlap corresponds to the short range attractive force between the peripheries of aggregates. The ionic strength of clusters is reduced in proportion to the degree of overlap. The consequence of the charge imbalance expressed by eqn (7) is thus amplified. This is accompanied by a long-range repulsion among aggregates, and the balance of these two effects determines cluster size in a manner discussed by Groenewold and Kegel[77] for dispersions of boehmite rods; by Stradner *et al.*[78] for a mixture of poly-12-hydroxystearic acid and spherical particles with poly(methylmethacrylate) cores; and by Bordi *et al.*[79] for a liposome–poly(acrylic acid) system. In our system, both ''surface tension'' forces and charge repulsion forces can increase with protein charge over the pH range studied, so that the relative volumes of dense and dilute domains need not be pH dependent. However the increased attraction among peripheries can result in greater longevity of clusters.

Conclusions

The techniques employed here probe the dynamics and structure of protein–polyelectrolyte coacervates on time scales from tens of nanoseconds to hundreds of seconds, and corresponding length scales from nm to μm. The relevant phenomena vary from polyelectrolyte segmental motion to migration of proteins over distances ranging over five orders of magnitude, but the unique features of the coacervates are related to the coexisting phases with heterogeneity in the range of hundreds of nm. This mesophase separation is manifested in several ways. (1) FRAP displays two modes of diffusion for a non-interacting probe, FITC-Ficoll. (2) Multiple diffusion modes are also seen in DLS, one of them remarkably similar to the fast Ficoll diffusivity from FRAP. (3) Regions of high contrast in cryo-TEM point towards domains of high protein concentration embedded in a continuous more dilute phase whose low density and high volume fraction facilitates the surprisingly rapid diffusivities seen by both DLS and FRAP.

The size of protein-rich domains suggested by cryo-TEM are in agreement with the average dimensions of 200–400 nm of scattering objects obtained by SLS Guinier plots. DLS indicates lifetimes of tens of ms or longer for these dense domains. The dependence of FITC-Ficoll diffusivities on the pH and ionic strength of coacervate preparation—both known from DLS and rheology to enhance the microscopic and macroscopic integrity of the samples—arises from the facilitation of Ficoll diffusion by the disintegration of the dense domains. The similarity of the overall fluorescence recovery time, *ca.* 200–400 s, to the elasticity recovery time of pre-sheared coacervates suggests that both are related to the lifetimes of the most durable dense domains. Taken together our results indicate that transient dense domains of high viscosity modulate the diffusion of proteins both by containment and obstruction.

Acknowledgements

Portions of this work were supported by NSF grant DMR0076068. We thank Nadia Edwin for her help with stripe bleaching FRAP measurements.

References

1 H. B. Bohidar, P. L. Dubin, P. R. Majhi, C. Tribet and W. Jaeger, Effects of protein–polyelectrolyte affinity and polyelectrolyte molecular weight on dynamic properties of bovine serum albumin–poly(diallyldimethylammonium chloride) coacervates, *Biomacromolecules*, 2005, **6**, 1573–1585.
2 D. J. Burgess and J. E. Carless, Microelectrophoretic studies of gelatin and acacia for the prediction of complex coacervation, *J. Colloid Interface Sci.*, 1984, **98**, 1–8.
3 C. G. de Kruif, F. Weinbreck and R. de Vries, Complex coacervation of proteins and anionic polysaccharides, *Curr. Opin. Colloid Interface Sci.*, 2004, **9**, 340–349.
4 C. Schmitt, C. Sanchez, S. Desobry-Banon and J. Hardy, Structure and Technofunctional Properties of Protein–Polysaccharide Complexes: A Review, *Crit. Rev. Food Sci. Nutr.*, 1998, **38**, 689–753.
5 S. L. Turgeon, M. Beaulieu, C. Schmitt and C. Sanchez, Protein–polysaccharide interactions: phase-ordering kinetics, thermodynamic and structural aspects, *Curr. Opin. Colloid Interface Sci.*, 2003, **8**, 401–414.
6 Y. Wang, K. Kimura, Q. Huang, P. L. Dubin and W. Jaeger, Effects of salt on polyelectrolyte-micelle coacervation, *Macromolecules*, 1999, **32**, 7128–7134.
7 H. Dautzenberg, Polyelectrolyte complex formation and highly aggregating systems: methodical aspects and general tendencies, in *Physical Chemistry of Polyelectrolytes*, ed. T. Radeva, Marcel Dekker, New York, 2001, pp. 743–792.
8 V. Ball, M. Winterhalter, P. Schwinte, P. Lavalle, J. C. Voegel and P. Schaaf, Complexation mechanism of bovine serum albumin and poly(allylamine hydrocolloid), *J. Phys. Chem. B*, 2002, **106**, 2357–2364.
9 P. A. Oparin, The Origin of Primary Colloidal Systems, in *The Origin of Life*, Dover Publ., New York, 1953, ch. VI, pp. 137–162.
10 F. Weinbreck, M. Minor and C. G. de Kruif, Microencapsulation of oils using whey protein/gum arabic coacervates, *J. Microencapsulation*, 2004, **21**, 667–679.
11 V. Ducel, J. Richard, P. Saulnier, Y. Popineau and F. Boury, Evidence and characterization of complex coacervates containing plant proteins: application to the microencapsulation of oil droplets, *Colloids Surf., A*, 2004, **232**, 239–247.
12 O. N. Singh and D. J. Burgess, Development of a novel method of microencapsulation for a model protein, β-glucuronidase, *Pharm. Sci.*, 1996, **2**, 223–228.
13 D. J. Burgess and S. Ponsart, β-Glucuronidase activity following complex coacervation and spray drying microencapsulation, *J. Microencapsulation*, 1998, **15**, 569–579.
14 Y. Jiang, Q. Huang, Microencapsulation and controlled-release of food enzyme using protein–polysaccharide coacervates, *Abstracts of Papers, 228th ACS National Meeting (Philadelphia, PA)*, 2004, American Chemical Society, Washington DC.
15 Y. Wang, J. Y. Gao and P. L. Dubin, Protein Separation *via* Polyelectrolyte Coacervation: Selectivity and Efficiency, *Biotechnol. Prog.*, 1996, **12**, 356–362.
16 J. Xia, K. Mattison, V. Romano, P. L. Dubin and B. B. Muhoberac, Complexation of trypsin and alcohol dehydrogenase with poly-(diallyldimethylammonium chloride), *Biopolymers*, 1997, **41**, 359–365.
17 P. L. Dubin, B. B. Muhoberac and J. Xia, *US pat.*, 583 4271, 1998.
18 Y. Wang, K. Kimura, P. L. Dubin and W. Jaeger, Polyelectrolyte-Micelle Coacervation: Effects of Micelle Surface Charge Density, Polymer Molecular Weight, and Polymer/Surfactant Ratio, *Macromolecules*, 2000, **33**, 3324–3331.
19 D. Leisner and T. Imae, Interpolyelectrolyte complex and coacervate formation of poly(glutamic acid) with a dendrimer studied by light scattering and SAXS, *J. Phys. Chem. B*, 2003, **107**, 8078–8087.
20 H. G. Bungenberg de Jong, Complex Colloid Systems, in *Colloid Science*, ed. H. R. Kruyt, Elsevier Publishing Company, Inc., Amsterdam, Netherlands, 1949, ch. X, pp. 335–432.
21 A. Veis and C. Aranyi, Phase Separation in Polyelectrolyte Systems. 1. Complex Coacervates of Gelatin, *J. Phys. Chem.*, 1960, **64**, 1203–1210.
22 A. Nakajima and H. Sato, Phase Relationships of An Equivalent Mixture of Sulfated Polyvinyl Alcohol and Aminoacetalyzed Polyvinyl Alcohol in Microsalt Aqueous-Solution, *Biopolymers*, 1972, **11**, 1345–1355.
23 R. Daniels and E. M. Mittermaier, Influence of pH Adjustment on Microcapsules Obtained from Complex Coacervation of Gelatin and Acacia, *J. Microencapsulation*, 1995, **12**, 591–599.
24 D. J. Burgess, Practical Analysis of Complex Coacervation, *J. Colloid Interface Sci.*, 1990, **140**, 227–238.
25 C. Remunan-Lopez and R. Bodmeier, Effect of formulation and process variables on the formation of chitosan–gelatin coacervates, *Int. J. Pharm.*, 1996, **135**, 63–72.
26 K. W. Mattison, I. J. Brittain and P. L. Dubin, Protein–Polyelectrolyte Phase Boundaries, *Biotechnol. Prog.*, 1995, **11**, 632–637.
27 K. Kaibara, T. Okazaki, H. B. Bohidar and P. L. Dubin, pH-Induced Coacervation in Complexes of Bovine Serum Albumin and Cationic Polyelectrolytes, *Biomacromolecules*, 2000, **1**, 100–107.

28 A. Veis, Phase separation in polyelectrolyte systems. III. Effect of Aggregation and Molecular Weight Heterogeneity, *J. Phys. Chem.*, 1963, **67**, 1960–1965.
29 M. Skepoe and P. Linse, Complexation, Phase Separation, and Redissolution in Polyelectrolyte-Macroion Solutions, *Macromolecules*, 2003, **36**, 508–519.
30 E. Kokufuta, H. Shimizu and I. Nakamura, Stoichiometric complexation of human serum albumin with strongly acidic and basic polyelectrolytes, *Macromolecules*, 1982, **15**, 1618–1621.
31 Y. Li, K. W. Mattison, P. L. Dubin, H. A. Havel and S. L. Edwards, Light scattering studies of the binding of bovine serum albumin to a cationic polyelectrolyte, *Biopolymers*, 1996, **38**, 527–533.
32 H. Sato and A. Nakajima, Formation of a polyelectrolyte complex from carboxymethyl cellulose and poly(ethylenimine), *Polym. J.*, 1975, **7**, 241–247.
33 C. Schmitt, C. Sanchez, S. L. Turgeon and J. Hardy, Complex coacervation between β-lactoglobulin and acacia gum in aqueous medium, *Food Hydrocolloids*, 1999, **13**, 483–496.
34 H. G. Bungenberg de Jong, Reversal of Charge Phenomena, Equivalent Weight and Specific Properties of the Ionized Groups, in *Colloid Science*, ed. H. R. Kruyt, Elsevier Publishing Company, Inc., Amsterdam, Netherlands, 1949, ch. IX, pp. 259–334.
35 L. S. Ahmed, J. Xia, P. L. Dubin and E. Kokufuta, Stoichiometry and the mechanism of complex formation in protein–polyelectrolyte coacervation, *J. Macromol. Sci., Pure Appl. Chem.*, 1994, **A31**, 17–29.
36 J. M. Park, B. B. Muhoberac, P. L. Dubin and J. Xia, Effects of protein charge heterogeneity in protein–polyelectrolyte complexation, *Macromolecules*, 1992, **25**, 290–295.
37 Y. Wang, Protein separation *via* association with confined polyelectrolytes: coacervation and chromatography, *PhD Thesis*, Purdue University, 1998.
38 F. Cousin, J. Gummel, D. Ung and F. Boue, Polyelectrolyte–Protein Complexes: Structure and Conformation of Each Species Revealed by SANS, *Langmuir*, 2005, **21**, 9675–9688.
39 X. Wang, Y. Li, Y. Lal and Q. Huang, Microstructure of β-Lactoglobulin/pectin complex coacervates studied by small-angle neutron scattering, *J. Phys. Chem. B*, 2007, **111**(3), 515–520.
40 L. Masaro and X. X. Zhu, Physical models of diffusion for polymer solutions, gels and solids, *Prog. Polym. Sci.*, 1999, **24**, 731–775.
41 B. Amsden, Modeling probe diffusion in aqueous polymer solutions, *Polymer*, 2002, **43**, 1623–1630.
42 G. D. J. Phillies, Self and Tracer Diffusion of Polymers in Solution, *Los Alamos Natl. Lab., Prepr. Arch., Condens. Matter*, 2004, arXiv:cond-mat/0403109.
43 R. Cong, E. Temyanko and P. S. Russo, Diffusion of Labeled Polyelectrolyte Probes in Unlabeled Polyelectrolyte Matrix Solutions, *Macromolecules*, 2005, **38**, 10627–10630.
44 R. Simson, B. Yang, S. E. Moore, P. Doherty, F. S. Walsh and K. A. Jacobson, Structural mosaicism on the submicron scale in the plasma membrane, *Biophys. J.*, 1998, **74**, 297–308.
45 H. Dautzenberg, E. Goernitz and W. Jaeger, Synthesis and characterization of poly(diallyldimethylammonium chloride) in a broad range of molecular weight, *Macromol. Chem. Phys.*, 1998, **199**, 1561–1571.
46 R. E. Crandall, J. Janatova and J. D. Andrade, The effects of radioiodination and fluorescent labelling on albumin, *Prep. Biochem.*, 1981, **11**, 111–138.
47 K. Luby-Phelps, Preparation of fluorescently labeled dextrans and Ficolls, *Methods Cell Biol.*, 1989, **29**, 59–73.
48 L. A. Mark, Modeling of glomerular basement membrane as a charged fiber-matrix, *PhD Thesis*, Indiana University, 2001.
49 F. S. Millett and L. M. Green, *Methods in Enzymology*, ed. M. R. Waterman and E. F. Johnson, Academic Press, San Diego, 1991, p. 716.
50 N. A. Busch, T. Kim and V. A. Bloomfield, Tracer Diffusion of Proteins in DNA Solutions. 2. Green Fluorescent Protein in Crowded DNA Solutions, *Macromolecules*, 2000, **33**, 5932–5937.
51 K. Jacobson, E. Wu and G. Poste, Measurement of the translational mobility of concanavalin A in glycerol–saline solutions and on the cell surface by fluorescence recovery after photobleaching, *Biochim. Biophys. Acta*, 1976, **433**, 215–222.
52 S. S. Jena and V. A. Bloomfield, Probe Diffusion in Concentrated Polyelectrolyte Solutions: Effect of Background Interactions on Competition between Electrostatic and Viscous Forces, *Macromolecules*, 2005, **38**, 10551–10556.
53 B. Fong, W. Stryjewski and P. S. Russo, On the Use of Pattern Fluorescence Photobleaching Recovery with Modulation Detection to Obtain Colloidal Size Distributions, *J. Colloid Interface Sci.*, 2001, **239**, 374–379.
54 P. S. Russo, J. Qiu, N. J. Edwin, Y.-W. Choi, G. J. Doucet, D. Sohn, Fluorescence Photobleaching Recovery, a Primer, in *Soft Matter: Scattering, Imaging and Manipulation*, ed. R. Pecora and R. Borsali, Springer, New York, NY, 2006.
55 T. Kawamoto, A. Hashidzume and Y. Morishima, Rheological behavior in water of complexes formed from poly(sodium 2-(acrylamido)-2-methylpropanesulfonate) and positively charged rodlike micelles, *J. Colloid Interface Sci.*, 2005, **286**, 142–147.
56 V. Agarwal, M. Singh, G. McPherson, V. John and A. Bose, Microstructure evolution in aqueous solutions of cetyl trimethylammonium bromide (CTAB) and phenol derivatives, *Colloids Surf., A*, 2006, **281**, 246–253.
57 Z. Bu and P. S. Russo, Diffusion of Dextran in Aqueous (Hydroxypropyl)cellulose, *Macromolecules*, 1994, **27**, 1187–1194.
58 R. Furukawa, J. L. Arauz-Lara and B. R. Ware, Self-diffusion and probe diffusion in dilute and semidilute aqueous solutions of dextran, *Macromolecules*, 1991, **24**, 599–605.
59 D. S. Banks and C. Fradin, Anomalous diffusion of proteins due to molecular crowding, *Biophys. J.*, 2005, **89**, 2960–2971.
60 R. Cong, E. Temyanko, P. S. Russo, N. Edwin and R. M. Uppu, Dynamics of Poly(styrenesulfonate) Sodium Salt in Aqueous Solution, *Macromolecules*, 2006, **39**, 731–739.
61 Y. A. Antonov and B. A. Wolf, Calorimetric and structural investigation of the interaction between bovine serum albumin and high molecular weight dextran in water, *Biomacromolecules*, 2005, **6**, 2980–2989.
62 H. B. Bohidar and P. L. Dubin, Protein–polyelectrolyte coacervates: gels or concentrated polymer solutions?, *Polym. Prepr. (Am. Chem. Soc., Div. Polym. Chem.)*, 2000, **41**, 698–699.
63 J. Sato and V. Breedveld, Transient rheology of solvent-responsive complex fluids by integrating microrheology and microfluidics, *J. Rheol.*, 2006, **50**, 1–19.
64 A. Hines and R. Maddox, *Mass Transfer: Fundamentals and Applications*, 1984, Prentice Hall, Englewood Cliffs, NJ, p. 500.
65 W. M. Deen, Hindered transport of large molecules in liquid-filled pores, *AIChE J.*, 1987, **33**, 1409–1425.
66 A. S. Verkman, Solute and macromolecule diffusion in cellular aqueous compartments, *Trends Biochem. Sci.*, 2002, **27**, 27–33.
67 H. B. Bohidar, Y. Lal and P. L. Dubin, unpublished work.
68 X. Feng and P. L. Dubin, unpublished work.
69 M. Girard, S. L. Turgeon and S. F. Gauthier, Thermodynamic parameters of beta-lactoglobulin-pectin complexes assessed by isothermal titration calorimetry, *J. Agric. Food Chem.*, 2003, **51**, 4450–4455.
70 D. Guzey and D. J. McClements, Characterization of β-lactoglobulin–chitosan interactions in aqueous solutions: a calorimetry, light scattering, electrophoretic mobility and solubility study, *Food Hydrocolloids*, 2005, **20**, 124–131.
71 N. Laugel, C. Betscha, M. Winterhalter, J. C. Voegel, P. Schaaf and V. Ball, Relationship between the Growth Regime of Polyelectrolyte Multilayers and the Polyanion/Polycation Complexation Enthalpy, *J. Phys. Chem. B*, 2006, **110**, 19443–19449.
72 J. Xia, P. L. Dubin, Y. Kim, B. B. Muhoberac and V. J. Klimkowski, Electrophoretic and quasi-elastic light scattering of soluble protein–polyelectrolyte complexes, *J. Phys. Chem.*, 1993, **97**, 4528–4534.
73 Y. Li, P. L. Dubin, H. A. Havel, S. L. Edwards and H. Dautzenberg, Complex Formation between Polyelectrolyte and Oppositely Charged Mixed Micelles: Soluble Complexes *vs* Coacervation, *Langmuir*, 1995, **11**, 2486–2492.
74 G. Mekhloufi, C. Sanchez, D. Renard, S. Guillemin and J. Hardy, pH-Induced Structural Transitions during Complexation and Coacervation of β-Lactoglobulin and Acacia Gum, *Langmuir*, 2005, **21**, 386–394.

75 M. Meyer, E. C. Le Ru and P. G. Etchegoin, Self-Limiting Aggregation Leads to Long-Lived Metastable Clusters in Colloidal Solutions, *J. Phys. Chem. B*, 2006, **110**, 6040–6047.
76 R. J. Allen and P. B. Warren, Complexation and Phase Behavior of Oppositely Charged Polyelectrolyte/Macroion Systems, *Langmuir*, 2004, **20**, 1997–2009.
77 J. Groenewold and W. K. Kegel, Anomalously large equilibrium clusters of colloids, *J. Phys. Chem. B*, 2001, **105**, 11702–11709.
78 A. Stradner, H. Sedgwick, F. Cardinaux, W. C. K. Poon, S. U. Egelhaaf and P. Schurtenberger, Equilibrium cluster formation in concentrated protein solutions and colloids, *Nature*, 2004, **432**, 492–495.
79 F. Bordi, C. Cametti and S. Sennato, Large equilibrium clusters in low-density aqueous suspensions of polyelectrolyte–liposome complexes: a phenomenological model, *Phys. Rev. E: Stat., Nonlinear, Soft Matter Phys.*, 2005, **71**, 050401-1–050401-4.

